4

Carbon-Bearing Phases throughout Earth's Interior

Evolution through Space and Time

VINCENZO STAGNO, VALERIO CERANTOLA, SONJA AULBACH, SERGEY LOBANOV, CATHERINE A. MCCAMMON, AND MARCO MERLINI

4.1 Introduction

Carbon (C) occurs in the mantle in its elemental state in the form of graphite and diamond, but also as oxidized compounds that include carbonate minerals and carbonated magmas, as reduced components such as methane and carbide, and as gaseous phases in the C–O–H chemical system. The occurrence of C-bearing phases characterized by different oxidation states reflects magmatic processes occurring in Earth's interior that link to its oxygenation through space and time.[1] Improving our understanding of the physical and chemical behavior of carbon at extreme conditions sheds light on the type and depth of possible reactions taking place in the interior of Earth and other planets over time and allows the identification of deep carbon reservoirs and mechanisms that move carbon among different reservoirs from the surface to the atmosphere, thereby affecting the total terrestrial budget of carbon ingassing and outgassing.

Carbon occurs in diverse forms depending on surrounding conditions such as pressure, temperature, oxygen fugacity (fO_2), and the availability of chemical elements that are particularly reactive with carbon to form minerals and fluids. Despite the low abundance of carbon within Earth,[2] the stability of C-rich phases in equilibrium with surrounding minerals provides an important geochemical tracer of redox evolution in Earth and other planets, as well as an important economic resource in the form of diamonds.

Knowledge of carbon cycling through the mantle requires an understanding of the stable forms of carbon-bearing phases and their abundance at pressures, temperatures, and fO_2 values that are representative of Earth's interior. Such information is necessary to identify potential carbon reservoirs and the petrogenetic processes by which carbon may be (re) cycled through the mantle over time, eventually being brought to the surface by magmas and to the atmosphere as dissolved gaseous species.

Accurate estimates of carbon abundance in Earth's interior are challenging for many reasons, such as the unknown primordial budget of carbon,[3] the low solubility of carbon in the dominant silicate minerals of the upper and lower mantle,[4–7] the low modal abundance of accessory carbon-bearing minerals and graphite/diamond in mantle xenoliths, and because magmas occurring at shallow depths are the product of igneous differentiation, magma chamber processes, and degassing. Experimental studies conducted at high

pressures and high temperatures help to constrain the initial carbon budget resulting from accretion and core–mantle differentiation processes. These estimates can then be used to determine the amount of carbon in the present-day terrestrial mantle by simulating possible reactions within simplified mantle mineral assemblages that identify the roles of pressure, temperature, and bulk chemistry on carbon speciation.

This chapter addresses fundamental questions about carbon within Earth: At which depths does carbon transform into different phases? How has the redox state of the mantle influenced carbon speciation throughout geological history? Are carbonate minerals more stable than diamonds or CO_2 fluids under certain conditions? Can minerals control the distribution of carbon within the mantle? Answers to these questions reveal how carbon has evolved in the mantle through time and where it may reside in the present-day mantle.

4.2 The Abundance, Speciation, and Extraction of Carbon from the Upper Mantle over Time

Estimates of carbon abundance in Earth's interior can be made through analysis of mantle rocks sampled as peridotitic and eclogitic xenoliths carried to the surface by successively erupted lavas, combined with experimental investigations of the carbon contents of synthetic liquids and minerals at upper- and lower-mantle pressures and temperatures. Carbon abundance in upper-mantle rock-forming minerals such as olivine, orthopyroxene, clinopyroxene, and garnet in equilibrium with carbonated magmas (Na_2CO_3, Ref. 4; olivine tholeiite with ~4 wt.% CO_2, Ref. 5) were shown to be in the range of a few ppm, as also detected in synthetic minerals representative of the transition zone and lower mantle (<1 ppm; Refs. 6 and 7). These findings highlight the extreme geochemical incompatibility of carbon and the role of magmas as its main carriers in space and time.

Experimental investigation of carbon solubility in magmas has revealed that most carbon is generally present as molecular CO_2 and CO_3^{2-} molecules. Their concentrations follow a linear positive trend with pressure and alkali content ($K_2O + Na_2O$) and show a negative correlation with SiO_2 from alkali basalts to rhyolites and the water content of the melt.[8] Among the diverse suites of effusive products, basaltic lavas that have erupted along mid-ocean ridges have dissolved CO_2 concentrations that are inherited from deep mantle source rock and can therefore be used to estimate the mantle abundance of CO_2. However, due to the low solubility of CO_2 in magmas during ascent and decompression, the possibility of tracking its history from the carbonated source rock to the surface is limited to few known undegassed lavas (e.g. Siqueiros and 2πD43 popping rocks). Using the observed correlation of undegassed CO_2 versus trace elements (e.g. Rb, Ba, and Nb) from olivine-hosted melt inclusions, LeVoyer et al.[9] determined a global average CO_2 content of 137 ± 54 ppm, corresponding to an average flux out of mid-ocean ridges (60,864 km length) of 1.8×10^{12} mol·yr^{-1}. This estimate pertains to a depleted mantle source, given that the carbon content of the bulk silicate Earth, generally determined from mantle plume-like magmas, is higher, ranging from 500 to 1000 ppm.[3] In addition, the LeVoyer value is

higher than the 72 ppm measured from Siqueiros melt inclusions by Saal et al.,[10] but much lower than the 1300 ± 800 ppm measured in the 1990s by Dixon et al.[11] on alkalic Atlantic lavas. Whether these carbon contents reflect those of the primordial mantle strongly depends on the origin of carbon, its initial budget at the time of Earth's accretion, and the petrological processes capable of mobilizing deep carbon.

Based on recent experimental studies, it was proposed that mantle carbon was inherited at the time of accretion from a Mercury-sized oxidized C-bearing S-rich body, which established the partitioning of carbon between the metallic core and silicate magma ocean during solidification of the terrestrial mantle.[12] An initially delivered carbon content ranging from 700 to 1000 ppm has been proposed for a reduced or S-rich impactor with a mass of 5–30% of Earth in order to match the current carbon concentration in the mantle. The mobilization of this primordial carbon, likely in the form of elemental carbon in Fe(Ni) alloys and CH_4 in the magma ocean as proposed by Li et al.,[12] links to the evolution of the mantle redox state over time. This issue remains controversial, however, and there is still an open debate on the different C species (CH_4, CO_2, and CO) that can be transported by mantle magmas (Ref. 8 and references therein).

Late addition of oxidized meteoritic bodies and enrichment of the post-core formation mantle in Fe_2O_3 consequent to the loss of Fe to the metallic core have been proposed, among a plethora of other processes, to explain the increase of fO_2 from conditions where C would be stable as diamond and in Fe(Ni) alloys ($fO_2 \approx$ iron–wüstite buffer (IW) – 2; Refs. 13 and 14) to conditions where C^{4+} is the dominant species incorporated in carbonate minerals and melts (IW + 1 < fO_2 < IW + 5). Geochemical tracers such as Ce in zircons believed to have crystallized in equilibrium with Hadaean magmas[15] and the V/Sc ratio of erupted continental basalts[16] have been used to argue in favor of a constant mantle redox state over the last 4.4 billion years at values where C^{4+} is stable, and therefore able to mobilize carbon as CO_2 and/or CO_3^{2-} dissolved in magmas. In contrast, based on the reconstruction of the mantle redox state over time using the V/Sc ratio of Archean spreading ridge-derived metabasalts, Aulbach and Stagno[17] found that the ambient mantle became gradually more oxidized by ~1.5 log units between ca. 3 Ga and 1.9 Ga, when fO_2 values similar to modern mid-ocean ridge basalts (MORBs) are recorded (Figure 4.1a). Figure 4.1b illustrates how a reduced asthenospheric Archaean mantle expected to host C in the form of diamond (or graphite) and CH_4 becomes more oxidized along a decompression path (Figure 4.1b, red line) as a result of the pressure effect on the equilibrium:[18]

$$4\,Fe^{3+}{}_{(bulk)} + C^0 = 4\,Fe^{2+}{}_{(bulk)} + C^{4+}{}_{(vap/melt/solid)}, \quad (4.1)$$

until the local fO_2 at which carbon turns into carbonate[19] is reached (fayalite–magnetite–quartz buffer (FMQ) – 2 log units; Figure 4.1b, blue line) at ~100 km depth. In Eq. (4.1), Fe^{3+} and Fe^{2+} refer to the ferric and ferrous iron of the bulk peridotite mantle rock, respectively. A similar equilibrium could be written to explain the distribution and fate of other important magmatic volatiles like H_2 and H^+, N^{3-} and N_2, and S^{2-} and S^{6+} in igneous systems dominated by Fe-bearing silicates, with dramatic implications for volcanic outgassing and atmospheric composition over time.

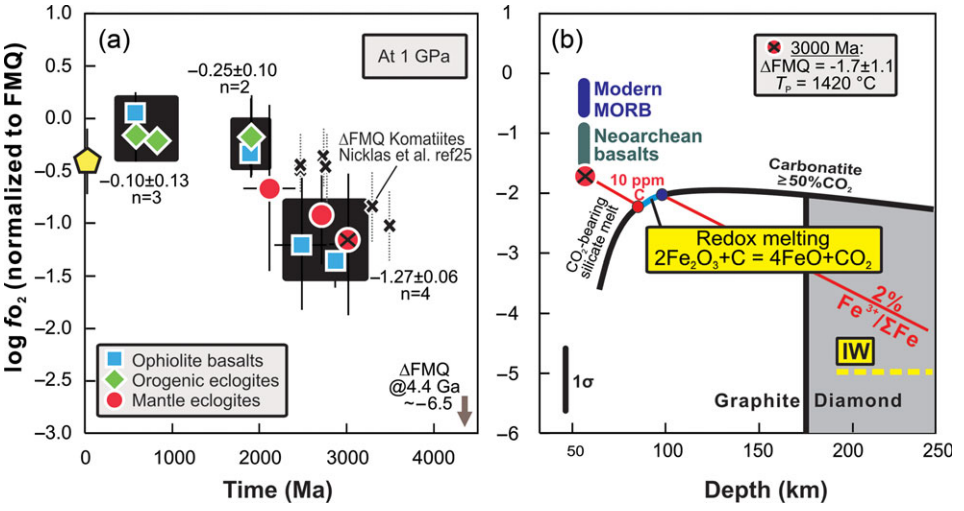

Figure 4.1 (a) fO_2 as a function of time calculated from V/Sc of mid-ocean ridge-derived basalts and metabasalts occurring in ophiolites, as orogenic eclogites, or mantle eclogites (data in Aulbach and Stagno[17]). fO_2 values were projected to 1 GPa to avoid bias due to deeper onset of partial melting in warmer ancient convecting mantle. Shown for comparison are results for komatiites from Nicklas et al.[25] (b) Thermodynamic prediction of the variation in the mantle oxidation state upon decompression, obtained using oxy-thermobarometry for garnet-bearing peridotite.[18] The graph shows the depth at which melting would occur as soon as 10 ppm C, expected in the Archean convecting mantle and hosted in diamonds, is oxidized to carbonate by the redox reaction shown. A source mantle with 2% Fe_2O_3 would generate a melt at the local temperature corresponding to the solidus of a carbonated peridotite that would have the fO_2 calculated for the igneous protolith of the Lace eclogite suite shown in (a) (after Aulbach and Stagno[17]).

At these depths, carbonate–silicate melts are likely to have formed by redox melting of graphite-bearing mantle at the near-constant fO_2 favored by hotter temperatures during the Archaean, until all carbon (~10 ppm in the case of reduced early Earth[20]) was oxidized. Upon further decompression, the Archaean mantle would have continued to become more oxidized until the oxidation state of Archean MORBs, represented by a metabasaltic eclogite suite from Lace in the Kaapvaal craton,[21] is reached below the spreading ridge. Given that redox melting – today as well as in the early mantle – requires the reduction of Fe_2O_3 (i.e. Eq. 4.1), the oxidation state of MORBs does not directly reflect the mantle oxidation state at the source, a concept introduced by Ballhaus and Frost[22] in 1994 when they proposed the oxidation of MORBs from a more reduced mantle source due to the coupling between C/carbonate reactions and Fe^{3+}/Fe^{2+} variations upon decompression as represented by Eq. (4.1). This was demonstrated in recent experiments where measured fO_2 values of synthetic MORBs appeared different from the fO_2 of the coexisting spinel-bearing peridotite rock source by up to ~3 log units.[23] Nevertheless, a gradual increase of Fe^{3+} in the bulk asthenospheric mantle over time has been corroborated by the finding of extremely low $Fe^{3+}/\sum Fe$ in

mantle eclogites, which is not correlated with indices of subsequent melt depletion,[24] as well as V-based estimates of fO_2 in komatiites, picrites, and basalts of various ages showing a clear trend in the Archaean that levels out at ca. 2 Ga.[25]

4.3 The Stability of Reduced and Oxidized Forms of Carbon in the Upper Mantle: Continental Lithosphere versus Convective Mantle

Thermodynamic prediction of the stable form of carbon in the upper mantle can be made using oxy-thermobarometry applied to mantle rocks such as peridotites and eclogites based on the relation between the ferric/ferrous iron ratio of minerals such as spinel and garnet and the buffering capacity of the host rocks. The decreasing fO_2 with depth shown in Figure 4.2 links to the volume change of the reactions used as oxy-thermobarometers[18,26,27] and suggests that the Archaean continental lithospheric mantle down to ~270 km in depth might have equilibrated with elemental carbon in the form of diamond or graphite, plus a small volume of CO_2-bearing melts varying from carbonatitic (Figure 4.2, blue line) to kimberlitic (Figure 4.2, red region) in composition. The fO_2 at which diamond and CO_2-bearing melts can coexist with peridotite and eclogite depends on the effects that temperature (the local geotherm) and the presence of water have on the equilibria:[19,26]

$$\underset{\text{enstatite}}{2\,Mg_2Si_2O_6} + \underset{\text{dolomite/melt}}{CaMg(CO_3)_2} = \underset{\text{diopside}}{CaMgSi_2O_6} + \underset{\text{olivine}}{2\,Mg_2SiO_4} + \underset{\text{diamond}}{2\,C} + 2\,O_2 \tag{4.2}$$

and

$$\underset{\text{dolomite/melt}}{CaMg(CO_3)_2} + \underset{\text{coesite}}{2\,SiO_2} = \underset{\text{diopside}}{CaMgSi_2O_6} + \underset{\text{diamond}}{2\,C} + 2\,O_2. \tag{4.3}$$

A direct sampling of deep carbon phases is represented by diamantiferous peridotite and eclogite of Archaean age (1–3% diamonds in the cratonic lithosphere),[28] while the observation of carbonated magmas of mantle origin, although predicted by experimental phase equilibria studies on synthetic carbonated peridotites and eclogites, appears quite rare (about 490 deposits)[29] due to a decreasing trend over time coupled to secular mantle cooling and late-stage fractionation and assimilation processes[30,31] that make these products difficult to identify. The decrease of fO_2 with depth in the case of eclogite is expected to result in carbonate minerals (or fluids) being reduced to diamond during subduction of a carbonated oceanic crust at variable depths through oxidation of coexisting garnet and clinopyroxene mineral phases[26] depending on the Fe^{3+} of the bulk rock.[26,32]

The Fe(Ni) precipitation curve (Figure 4.2, orange line) marks the fO_2 conditions at which diamonds and Fe(Ni) alloys might coexist, therefore promoting the diffusion of carbon into adjacent metal or the formation of Fe(Ni)C intermetallic compounds depending on the local Fe(Ni)/C ratio.[33,34]

The extent to which the redox state of the continental mantle resembles that of the convective mantle is highly debated. The model proposed in Figure 4.1b is based on

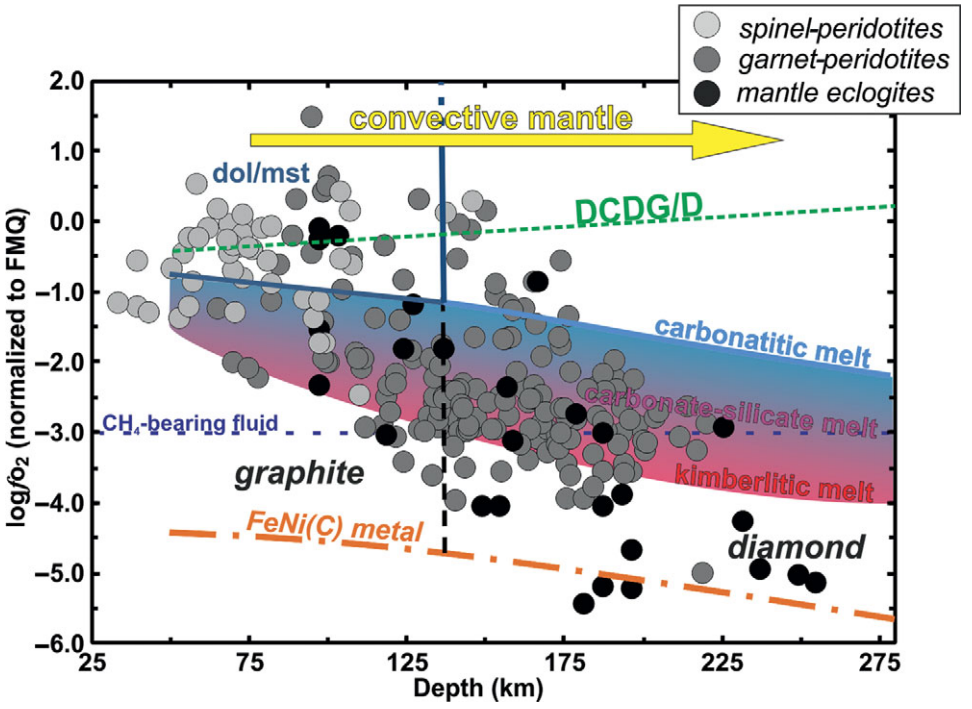

Figure 4.2 Log fO_2 (normalized to the FMQ buffer) determined for peridotitic and eclogitic xenoliths using oxy-thermobarometry for spinel/garnet peridotite and eclogite.[18,26,27] The blue curve is the fO_2 calculated for Eq. (4.2) along a cratonic geotherm of 40 $mW \cdot m^{-2}$ that defines the stability field between diamond (or graphite) and solid (liquid) carbonate within peridotite rocks. The orange curve indicates where Fe–Ni metallic alloys (with some C) are stable. The green line indicates the fO_2 buffered by Eq. (4.3) (see text).[26,35] CO_2-bearing silicate melts are stable at lower fO_2 values than carbonatitic melts in equilibrium with diamantiferous peridotite due to the temperature effect on Eq. (4.1).[18] The yellow arrow indicates the proposed oxidation state of a convective mantle contaminated by variable volumes of subducted carbonated lithologies.[37] DCDD/G = dolomite–coesite–diopside–(diamond/graphite).

conservative estimates in which a bulk silicate Earth composition[36] is used as an analogue for the asthenospheric mantle. For this case, the convective mantle is predicted to follow an fO_2 trend similar to the one in Figure 4.2 for natural mantle peridotites along a decompression path. This model might apply to a convective early Earth mantle not equilibrated with subducted lithologies. However, correlations between geochemical tracers such as CO_2 versus Nb and Ba measured in modern natural oceanic basalts suggest a different trend. These correlations were used to constrain mixing models of two components: a residual mantle peridotitic partial melt plus graphite-saturated partial melts of subducted lithologies (e.g. pyroxenite, MORB-eclogites, sediments) in different proportions. These models, supported by melting experiments, show that generation of CO_2-rich basalts of up to ~6 wt.% in the melt like those from Atlantic popping rocks[37] requires the contribution of

subduction-related melts originating from partial melting occurring in the carbonate stability field ($fO_2 \geq$ FMQ – 1; DCDD/G in Figure 4.2) rather than graphite/diamond-saturated sources. This results in a contaminated convective present-day mantle that is more oxidized than the Archaean continental lithospheric mantle (Figure 4.2).

4.4 The Redox State and Speciation of C in the Transition Zone and Lower Mantle

4.4.1 Carbides and C in (Fe,Ni) Alloys

In contrast to the top of the upper mantle, gaining knowledge of the redox state of the deeper upper mantle (300 km and below) is more challenging due to the lack of rocks that can be sampled at the surface. Previous experimental studies,[38,39] recently supported by observations of 53 sublithospheric natural diamonds (termed CLIPPIR due to their Cullinan-like large size, rare occurrence of inclusions, relatively pure nature, and irregular shape and resorption features),[40] provide evidence of C-bearing Fe metal occurring at the pressures of the transition zone and lower mantle. This observation would limit the stability of carbon to diamond and carbide phases, which is also supported by the discovery of Fe (Ni)/C alloys trapped in diamonds.[40–43] At the base of the upper mantle, the fO_2 at which Fe-carbides (e.g. Fe_3C and Fe_7C_3) would be stable in equilibrium with mantle silicates requires either extremely reducing conditions (~7 log units below the FeNi precipitation curve; orange line in Figure 4.2) or coexistence with olivine and orthopyroxene that is more enriched in ferrous iron[44] than would be expected for peridotite. In addition, the Fe–Ni–C solidus temperature ranges between 1150 and 1250°C at 10 GPa,[34] which is low compared to generally agreed cratonic geotherms. It is likely, therefore, that Fe–Ni–C alloys are either: (1) stable as molten phases;[34] (2) limited in their formation to the grain scale as a result of interaction with surrounding C-saturated reduced fluids;[44] or (3) result from solid–solid reactions between preexisting Fe–Ni alloys and subducted carbon (carbonate or diamond) of particularly cold slabs.[45] In the deep mantle, carbides can be stable in the form of molten Fe_7C_3 along with coexisting diamonds[33] if C is locally more abundant (>~100 ppm) than Fe. Interestingly, the presence of 100–200 ppm of sulfur in the Fe–Ni–C system at high pressures and temperatures was shown to prevent the formation of carbides and promote precipitation of diamonds even in particularly C-poor (5–30 ppm) regions of the deep mantle,[46] thus explaining the occurrence of Fe–Ni–S phases trapped in diamonds.[40]

4.4.2 Carbonate Minerals in Earth's Interior

In contrast to the view that bulk mantle redox conditions are reduced at transition-zone and lower-mantle depths, inclusions hosted in super-deep (sublithospheric) diamonds have also shown the presence of solid carbonates.[47,48] These observations raise important questions: (1) Do these inclusions reflect local fO_2 heterogeneities of the deep mantle? (2) What

transformations do solid carbonates experience to preserve their stability at high pressures and temperatures to act as main carbon hosts? The latter question links to the possibility that the fO_2 of the transition zone and lower mantle could be buffered by an influx of oxidized carbon in the form of solid carbonate, but questions remain as to which carbonates these might be. The speciation of carbon at conditions from the upper to the lower mantle, whether in the form of diamond or carbonate (either liquid or solid), has been a focus of investigations over the last decades. All experimental studies and theoretical calculations suggest that solid carbonates (i.e. the end members $CaCO_3$, $MgCO_3$, $FeCO_3$, and their solid solutions) are stabilized at conditions of Earth's lower mantle through a series of high-pressure phase transitions that are summarized below. This conclusion is also supported by the observations of extremely low solubility of carbon in deep mantle silicates such as wadsleyite, ringwoodite, bridgmanite, and ferropericlase in experimental studies conducted at high pressures and high temperatures.[6,7]

4.4.2.1 Dolomite and Its High-Pressure Polymorphs

It is generally accepted that dolomite, $CaMg(CO_3)_2$, is the dominant carbonate mineral up to about 4 GPa within simplified $CaO–MgO–Al_2O_3–SiO_2 + CO_2$ igneous systems, and is then replaced in dominance by magnesite at higher pressures.[49] However, both the bulk Ca/(Ca + Mg) ratio of the rock and the presence of a small amount of Fe in the structure that reduces the cation-sized misfit between Ca and Mg may play important roles in stabilizing high-pressure polymorphs at the conditions of Earth's lower mantle. Upon compression at ambient temperature, the rhombohedral dolomite structure is stable up to 17 GPa.[50] Above this pressure, a transition to dolomite-II with triclinic symmetry is observed with no observable volume change. Dolomite-II is stable upon heating to 1500 K;[51] however, it decomposes between 2000 and 2400 K below 35 GPa to form a mixture of oxides and diamond.[52] Dolomite-II is stable up to 35 GPa, whereupon a second phase transition is observed to triclinic dolomite-III.[51,52] Heating dolomite-III above 35 GPa to its melting point without evidence of decomposition demonstrates that dolomite-III can be a stable C-bearing mineral at Earth's mantle conditions. Theoretical computations indicate that dolomite transforms into a ring-carbonate structure at 115 GPa and 2500°C that features tetrahedrally coordinated carbon and threefold carbonate rings,[53] as shown in Figure 4.3.

In a recent experimental study conducted using a laser-heated diamond anvil cell, Dorfman and coauthors[54] explored chemical reactions occurring at the boundary between dolomite and Fe metal to simulate subducted carbonates penetrating the reduced lower mantle saturated in Fe metal (about 1 wt.%[38]) at ~51–113 GPa and 1800–2400 K. Their results suggest that the $MgCO_3$ component of subducted crustal dolomite would react with iron metal to form a mixture of diamond + Fe_7C_3 + ferropericlase, while $CaCO_3$ with a post-aragonite structure would be preserved. This study supports previous experimental observations on the formation of diamond + carbide by reduction of subsolidus carbonates,[45] and it demonstrates the potential role of dolomite as a deep carbon reservoir. So far,

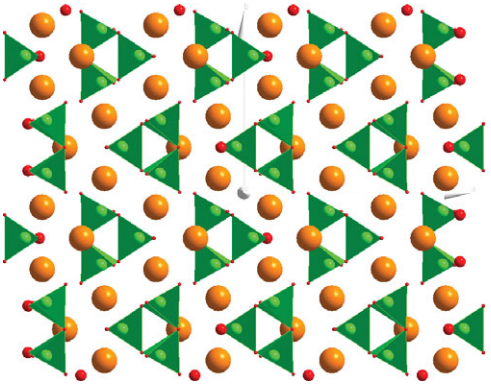

Figure 4.3 Crystal structure of dolomite-IV based on experimental single-crystal X-ray data collected in a diamond anvil cell at 115 GPa after annealing at 2500°C. The structure is based on threefold-ring carbonate units, with carbon in tetrahedral coordination.

however, its transport to the lower mantle appears limited to exotic Ca-rich, Si-poor thick portions of the oceanic slab, likely related to the subduction of sedimentary lithologies.[55]

4.4.2.2 Deep Carbon Stored as $CaCO_3$-like Phases

Calcite (the rhombohedral form of $CaCO_3$) and aragonite (orthorhombic $CaCO_3$) undergo a series of structural transitions toward denser phases with increasing pressure. Above 15 GPa, a new calcite polymorph, $CaCO_3$-IV, was discovered that shows stability at least up to 40 GPa.[56] The density of $CaCO_3$-IV is higher than aragonite (3.78 g/cm^3 at 30.4 GPa), which suggests that it might replace aragonite at intermediate mantle depths.[56] At pressures of more than ~40 GPa, $CaCO_3$ undergoes yet another phase transition into a so-called post-aragonite phase.[57] Compression to pressures of more than ~100 GPa leads to a different polymorph with a pyroxene-like structure based on CO_4 groups with sp^3-hybridized carbon.[57–60] Chemical bonding in sp^3-carbonates is different from bonding in carbonates based on sp^2-hybridized carbon; thus, sp^2–sp^3 crossover, if it occurs in mantle carbonates, may disrupt the silicate–carbonate chemical equilibrium. To date, however, the geochemical and geophysical consequences of sp^2–sp^3 transitions are not well understood. It is noteworthy, however, that calcite was found as an inclusion in a sublithospheric diamond,[47] confirming its stability in the lower mantle as a potential carbon reservoir and candidate for potential redox reactions through which diamond itself could form.

4.4.2.3 Magnesite and Fe-Bearing Solid Solutions as Deep Carbon Reservoirs

Magnesite and ferro-magnesite solid solutions have been found to occur as inclusions in diamonds that likely originated in Earth's lower mantle.[48] Despite the lack of evidence of siderite inclusions hosted in such super-deep diamonds, the role of iron in the stability of Fe-carbonates appears relevant in the mid-lower mantle, where spin crossover of Fe^{2+} from high spin (HS) to low spin (LS) changes the physical and chemical properties of

these carbonates,[61–63] with important implications for their seismic detectability (discussed below).

Magnesite remains stable at up to 100 GPa and 2200 K without decomposition or associated phase transformations.[64] Congruent melting of magnesite was reported between 2100 and 2650 K at pressures between 12 and 84 GPa, whereas decomposition to MgO and diamond was observed only above ~3000 K at similar pressures.[65] Isshiki et al.[64] first reported the transformation of magnesite to its high-pressure polymorph, magnesite-II, at ~115 GPa and ~2200 K. Maeda et al.[66] discussed phase relations in the $MgCO_3$–SiO_2 system up to 152 GPa and 3100 K. They reported a reaction between $MgCO_3$ phase II and SiO_2 ($CaCl_2$-type SiO_2 or seifertite) to form diamond and $MgSiO_3$ (bridgmanite or post-perovskite) at deep lower-mantle conditions via the following possible reaction:

$$SiO_2 + MgCO_3 \rightarrow MgSiO_3 + C + O_2, \tag{4.4}$$

indicating that CO_2 dissociates above ~33 GPa and at >1700–1800 K to form diamond plus free oxygen and bridgmanite. These results describe a possible mechanism of formation of super-deep diamond in cold slabs descending into the deep lower mantle resulting from the instability of magnesite phase II in the presence of exotic assemblages.

The physical and chemical properties of Fe-bearing carbonates, such as their density, Fe content, elasticity, and optical properties, may have important geological consequences. Melting of $FeCO_3$ was investigated experimentally at high pressures and temperatures equal to or above the terrestrial geotherm. Experiments indicate that iron carbonates melt incongruently up to ~70 GPa and at >2000 K to produce a minor quenched Fe^{3+}-rich phase and CO_2 in the liquid.[67,68] At higher pressures and similar temperatures, new carbonates were observed with tetrahedral C_3O_9 rings.[69] Merlini et al.[70] reported the transformation of Mg-siderite at pressures and temperatures corresponding to the top of the D´´ layer (i.e. ~135 GPa and ~2650 K), with formation of $Mg_2Fe^{(III)}{}_2(C_4O_{13})$ and a new oxide phase, $Fe_{13}O_{19}$, thus demonstrating that self-oxidation–reduction reactions can preserve carbonates in Earth's lower mantle to 2500 km in depth.

When slabs penetrate the lower mantle, redox reactions take place between the hotter outer part of the slab and the surrounding bulk mantle in order to balance the high Fe^{3+} content of bridgmanite (~80% in equilibrium with magnesite and diamonds),[71] similar to Eq. (4.1). The origin of diamonds in the lower mantle might be therefore linked to redox reactions involving Fe^{3+}-bearing minerals, which could also account for the high proportion of ferropericlase in lower-mantle diamond inclusions.[72] At greater depths, the high degree of trivalent iron incorporation into high-pressure carbonate structures and iron oxides can influence redox processes in the deep mantle, where changes in fO_2 could be buffered by the activity of carbon (Eq. 4.5) or oxygen (Eq. 4.6) rather than being controlled by charge balance between iron cations.

$$4\ FeCO_3 = Fe_4C_3O_{12} + C, \tag{4.5}$$

$$8\ Fe_4C_3O_{12} = 6\ Fe_4C_4O_{13} + 4\ Fe_2O_3 + 3\ O_2. \tag{4.6}$$

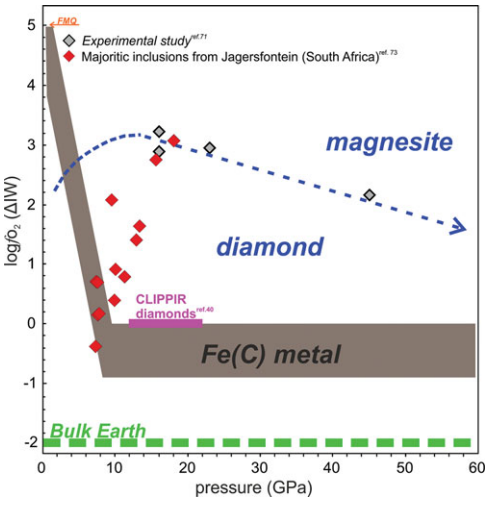

Figure 4.4 fO_2 stability of carbon phases at high pressures based on experimental studies,[71] as well as majorite inclusions in diamonds[73] and metal-bearing "CLIPPIR" diamonds.[40] The blue dashed line indicates the fO_2 values at which diamonds and carbonate (magnesite) are in equilibrium.[71]

4.4.3 Toward Oxy-Thermobarometry of the Deep Mantle and Implications for Carbon Speciation

Through the number of redox reactions that can be written to explore the mechanisms of diamond formation in the transition zone and lower mantle, a fundamental question arises: Is the deep mantle intrinsically buffered by abundant Fe-bearing minerals similarly to the upper mantle? A recent estimate of the deep-mantle redox state was proposed by Kiseeva et al.,[73] who measured the ferric iron content of majorite inclusions and developed an oxy-thermobarometer based on the self-redox capacity of majorite as a function of pressure. Figure 4.4 shows the fO_2 values calculated using Eq. (4.7):

$$2\ Ca_3Al_2Si_3O_{12} + 4/3\ Fe_3Al_2Si_3O_{12} + 2.5\ Mg_4Si_4O_{12} + O_2 = 2\ Ca_3Fe_2Si_3O_{12} + 10/3\ Mg_3Al_2Si_3O_{12} + 4\ SiO_2, \quad (4.7)$$

from majoritic inclusions in super-deep diamonds from the Jagersfontein kimberlite (South Africa).[74] The carbon/carbonate equilibrium buffer[71] refers to experimental measurements of the fO_2 at which diamond and magnesite coexist with transition-zone (wadsleyite/ringwoodite and clino-enstatite) and lower-mantle (bridgmanite and ferropericlase) mineral phases.[71] The results indicate the heterogeneity of mantle fO_2 in the transition zone, varying from about IW to IW + 3, where the high concentration of Fe^{3+} in majorite (between 8% and 30%) is linearly correlated with pressure and likely related to the oxidizing effect of CO_2-rich fluids rather than FeO disproportionation. This suggests that carbonate is, at least locally, a stable phase in Earth's deep mantle, stabilized at an fO_2 value about 2 log units above the iron–wüstite buffer. Carbonate could therefore participate

in melting processes depending on the local geotherm and promote carbon mobility through the formation of carbonatitic to kimberlitic melts. At higher pressures, ferropericlase and bridgmanite are expected to play major roles in buffering redox conditions through chemical reactions that involve the Fe^{3+}-bearing mineral end members. However, the crystal chemistry of these phases has been shown to be extremely complex due to simultaneous element substitution in different sites.[75]

4.5 Seismic Detectability of Reduced and Oxidized Carbon in Earth's Mantle

The presence of carbon within the mantle may be detectable using seismic data. A recent multidisciplinary study conducted by Garber and coauthors[28] showed that diamondiferous lithologies may be responsible for elevated shear-wave velocities (V_S; $\geq$4.7 km/s) detected at 120–150-km depths in cratonic lithospheric mantle. Diamond and eclogite (known to contain higher concentrations of diamond compared to peridotite)[35] are the most likely high-V_S candidates that could explain the observed seismic anomalies, implying the presence of up to about 3 vol.% diamond, depending on the peridotite and eclogite compositions and the local geotherm.

The seismic detectability of carbonates in the upper mantle and transition zone is related primarily to their crystal structure. Sanchez-Valle et al.[76] measured the elastic tensor of $Mg_{1-x}Fe_xCO_3$ with four compositions extending from pure magnesite to pure siderite using single-crystal Brillouin scattering spectroscopy at ambient conditions. They found that Fe substitution has a negligible effect on the adiabatic bulk modulus, K_S, of Mg–Fe carbonates, whereas the shear modulus, μ, decreases by 34% from $MgCO_3$ to $FeCO_3$. They concluded that, based on current seismic resolution (with a threshold of 2%), detection of carbonated regions from seismic velocity contrast would require high carbonate contents (~15 wt.% CO_2) in eclogite and >20 wt.% CO_2 in peridotite. These results are supported by the work of Yang et al.,[77] who measured the full elastic stiffness tensor of $MgCO_3$ up to 14 GPa at ambient temperature and up to 750 K at ambient pressure using Brillouin scattering in the diamond anvil cell.

In Fe-bearing carbonates, the pressure-induced splitting of iron 3d energy levels into two leads to the possibility of two different spin configurations for Fe^{2+}: (1) the HS state with four unpaired and two paired electrons; and (2) the LS state with six paired electrons. The spin pairing of electrons causes a volume collapse of the iron atomic volume, followed by shrinking of the octahedral site and ultimately of the unit cell. The first experimental observation of the HS–LS transition of Fe^{2+} in siderite was reported by Mattila et al.[78] using X-ray emission spectroscopy. They observed the transition to occur at ~50 GPa and at ambient temperature in natural siderite powder. Subsequent experimental and theoretical work provided further evidence of the spin transition in Fe-carbonates at ~45 GPa, as well as insights into how the spin transition affects the physical and chemical properties of carbonates.[79–86]

The spin transition causes changes in the thermoelastic properties of carbonates and may enhance the seismic detectability of carbon in the lower mantle. Liu et al.[87] observed

anomalous thermoelastic behavior in natural magnesiosiderite at high pressure and high temperature across the spin transition, including a dramatic increase in the thermal expansion coefficient and decreases in the isothermal bulk modulus and the bulk sound velocity by 75% and 50%, respectively. When compared to $MgCO_3$ at relevant pressure–temperature conditions of subducted slabs, HS magnesiosiderite with 65 mol.% $FeCO_3$ is approximately 21–23% denser and its unit-cell volume is 2–4% larger, whereas the LS state is 28–29% denser and 2% smaller than end-member magnesite. These results indicate that dense LS ferromagnesite can become more stable than HS ferromagnesite at pressures above ~50 GPa, providing a mechanism for (Mg,Fe)-bearing carbonate to be a major carbon host in the deeper lower mantle. Fu et al.[88] measured the full elastic stiffness tensor of $Mg_{0.35}Fe_{0.65}CO_3$ up to 70 GPa at ambient temperature using Brillouin light scattering and impulsive stimulated light scattering in a diamond anvil cell. They observed a dramatic softening of the C_{11}, C_{33}, C_{12}, and C_{13} moduli and stiffening of the C_{44} and C_{14} moduli across the spin transition in the mixed spin state. Outside the region of the spin transition, they observed a linear increase of all elastic moduli with pressure. Based on their work, mixed spin-state ferromagnesite is expected to exhibit abnormal elasticity in the mid-lower mantle, including a negative Poisson's ratio and a drastically reduced compressional wave velocity (V_P). Similar results were obtained by Stekiel et al.,[89] who determined the elastic stiffness moduli of $FeCO_3$ across the spin transition up to 60 GPa and at ambient temperature by inelastic X-ray scattering and density functional theory calculations. Based on calculations employing a pyrolitic mantle model and considering varying amounts of $Mg_{1-x}Fe_xCO_3$, the presence of magnesioferrite solid solutions changed the V_S more than the V_P. At least 3 vol.% of $FeCO_3$ would be needed to produce a shear velocity contrast of more than 1% due to the spin transition, and 8 vol.% of $Mg_{0.85}Fe_{0.15}CO_3$ would be needed to produce the same contrast between carbonated and non-carbonated pyrolitic mantle.

Our knowledge of the iron spin state of $FeCO_3$ is limited to near-room temperature conditions, as probing different electronic structures at combined high pressure–temperature conditions is challenging. Temperature broadens the pressure range of the HS to LS transition, but the depth range over which spin transitions take place remains uncertain (Figure 4.5). In addition, siderite is unstable at greater than ~1500 K (greater than ~40 GPa) and decomposes into iron oxides and C-bearing phases. As a result, $FeCO_3$ is unlikely to occur in the lower mantle at depths greater than ~1200 km. Instead, solid solutions involving iron oxides and sp^3-bonded novel Fe-carbonates ($Fe_4C_4O_{13}$ and $Fe_4C_3O_{12}$) may be the most common carbon-bearing phases at sufficiently oxidizing conditions.

4.6 Conclusion

In contrast to the immobile behavior of carbon in the Archaean lithospheric mantle, the deep carbon cycle in modern Earth linked with carbon transport through the convective mantle at varying pressure–temperature–fO_2 conditions over time shows evidence of large

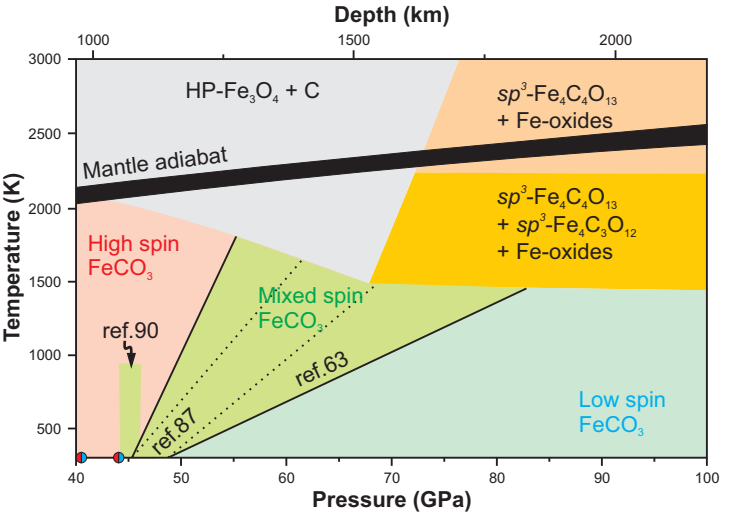

Figure 4.5 Stability and spin-state diagram of $FeCO_3$ at high pressure–temperature. Mixed blue–red circles depict the spin transition pressure in siderite at 300 K as observed in a soft pressure medium (e.g. Ne) at 40.5 GPa and in more rigid media (KCl, Ar, etc.) at ~44 GPa. Pink and blue regions are high and low spin-state regions, respectively. The pressure–temperature conditions of mixed-spin iron (0.1–0.9 LS) in $FeCO_3$ are uncertain (shown by different green-shaded areas). High-temperature transformations in the $FeCO_3$ system are shown after Cerantola et al.[67]

heterogeneities in mantle redox state, both vertically and laterally, which likely result from the contribution of subducted lithologies with varying degrees of oxidation through space and time. We conclude that the movement of carbon over geologic time is fundamentally controlled by the level of oxygenation of Earth's interior, which causes elemental carbon to oxidize to CO_2-bearing magmas, whose rheology mainly controls their transport properties.[91,92] The observation of both oxidized carbon and metal trapped as inclusions in sublithospheric diamonds testifies to the heterogeneity of mantle fO_2, thereby implying the stability of carbon in various redox states and phases (mineral, melt, or fluid), and even favored by the presence of additional elements like sulfur. The relation between iron oxidation state in mineral inclusions in diamonds and fO_2 is an important tool for determining the local redox conditions needed to model carbon speciation. Fluids in equilibrium with reduced mantle regions would be methane dominated and may precipitate diamonds by reduction of Fe, liberating water that could induce partial melting. On the other hand, the possible presence of carbonate as a source of carbon in natural diamond-forming processes is supported by experimental studies at high pressure and temperature that demonstrate the stability of diverse geologically relevant carbonates (and their solid solutions) such as magnesite, calcite/aragonite, and siderite down to the lower mantle. Redox reactions of these carbonates with Fe-bearing minerals in the bulk mantle under initially reducing conditions have been demonstrated to promote the formation of diamond as well as the crystallization of carbide phases, leading to mantle oxidation. Such

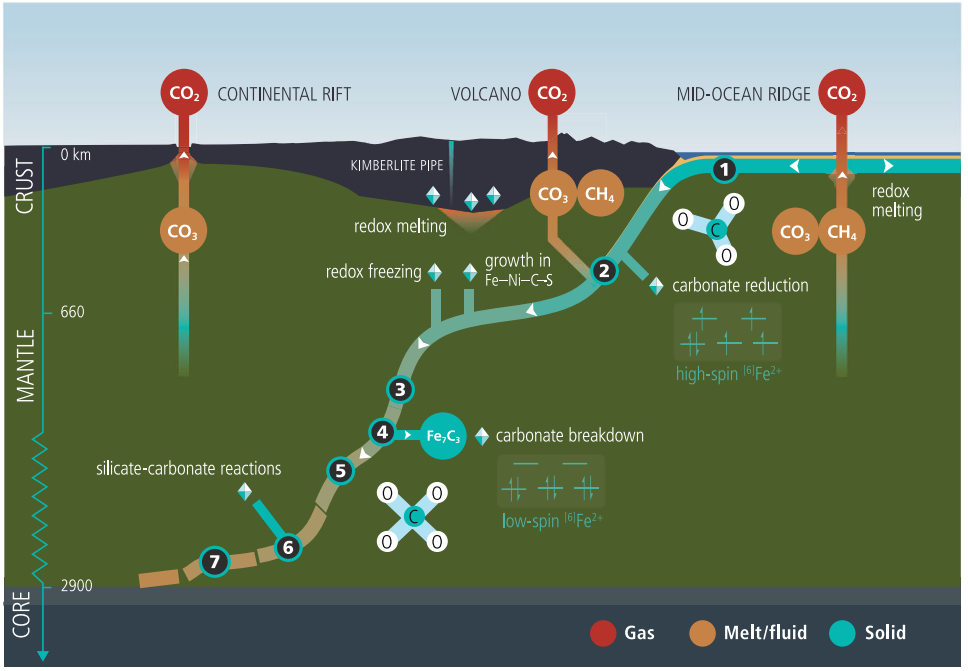

Figure 4.6 Simplified cartoon showing the distribution and forms of carbon inside Earth. Carbon has low solubility in mantle minerals;[4–7] hence, it occurs primarily in the form of gas (red circles), fluids or melts (orange circles), and accessory solid phases (green circles), including diamonds (octahedra). Reactions involving carbon include redox melting (diamond consuming) and freezing (diamond producing),[17,18] reduction of carbonate to diamond,[26,32] growth of diamond from metallic liquids,[33,34,40,46] breakdown of carbonate under reduced conditions,[45,54,66] redox reactions that produce tetracarbonates,[67,69] and reactions between carbonate and silicate.[66,71] Numbers indicate the depth at which important phase transitions in carbonates have been proposed to occur: (1) calcite to aragonite,[49] (2) dolomite to dolomite-II,[50,52] (3) aragonite to post-aragonite,[57] (4) dolomite-II to dolomite-III,[51,52] (5) Fe-carbonate to Fe-tetracarbonate,[67,69] (6) post-aragonite to $CaCO_3$ with sp^3-hybridized carbon,[57–60] and (7) magnesite to magnesite-II.[64] Ferrous iron in carbonate undergoes a HS to LS transition in the mid-mantle.[78–90] The thickness of the crust and slab is vertically exaggerated for clarity.

"conditioned" mantle regions may eventually allow carbonated melts and fluids to be mobilized along ascending (plumes) or descending (slabs) redox fronts, facilitating melt-mediated carbon transfer between different terrestrial reservoirs. Finally, elemental carbon transported upwards in upwelling mantle regions will be subjected to redox melting upon oxidation due to decompression. The resulting carbonated melts eventually erupt at the surface, where they interact with the hydrosphere and atmosphere. Figure 4.6 summarizes the stability of different carbon species through space and (indirectly) time with a particular focus on the asthenospheric mantle, the continental lithosphere, and subducted slabs.

4.7 Limits to Knowledge and Unknowns

Although great advances have been made, important limits to knowledge remain regarding the stability and mobility of carbon-bearing phases and their interaction with silicates and metals at pressure–temperature–fO_2 conditions relevant to the deep Earth. Redox melting and freezing reactions, as a function of fO_2, are critical in mediating transitions between the relatively refractory forms of carbon, such as diamond/graphite, carbide, and metal alloys, to highly mobile oxidized forms, such as carbonated melts and CO_2-bearing fluids.[18,93,94] However, the amount of carbon involved in these reactions, the participating minerals, and the fO_2 in the mantle with depth and through time remain highly uncertain. This uncertainty arises because most of our knowledge relies on indirect estimates based on mostly degassed magmas and direct estimates from mantle xenoliths and diamonds entrained in magmas that are irregularly distributed in space and time. Moreover, mantle xenoliths and diamonds are exclusively or dominantly derived from the lithospheric mantle and may sample multiply reactivated fluid and melt pathways that are not representative of the lithospheric mantle and even less so of the convective mantle.[95] The few sublithospheric diamonds available for study sample anomalous mantle domains characterized by strong compositional and redox gradients at the interface between deeply subducted slabs and ambient mantle.[93,96] Thus, although it is assumed that the fO_2 of the metal-saturated mantle below ~250–300 km in depth is effectively buffered close to the iron–wüstite redox buffer (where carbonates and carbonated melts are unstable[94]), sublithospheric diamonds appear to record much higher fO_2 values, linked to the influx of slab-derived oxidizing agents.[73] In addition, the CO_2 content of oceanic basalts has been suggested to require carbonated redox melting rather than graphite-saturated melting, implying higher fO_2 values than are inferred from lithospheric mantle xenoliths.[37] The problem of constraining the dominant fO_2 and redox equilibria with depth is only exacerbated in deep time, where debate over appropriate sample material and redox proxies continues.[15–17,98]

Progress on deciphering the speciation and distribution of carbon in modern Earth's interior will be made by combining observations from experiments and theoretical studies with increasingly sophisticated remote-sensing tools. For example, the ponded products of redox melting may be increasingly traceable by geophysics due to the increasingly well-characterized melting relations of carbon-bearing mantle[99] and constraints on the physical properties of carbonated melts (e.g. viscosity, seismic velocity, and electrical conductivity),[91,92,98] and they have indeed been linked to low-velocity zones below the oceanic lithosphere.[100] The fate of carbonates in subducting slabs, however, remains poorly constrained, in part due to the unknown variation of mantle fO_2 with depth and time. Carbonates do show rich polymorphism at high-pressure, high-temperature conditions, which renders them stable along the geotherm. Therefore, studies that explore the interaction of carbonates with silicates at well-controlled pressure, temperature, and redox conditions will provide important insights into the survival and mobility of oxidized carbon species in the mantle. Recent advances in experimental design that allow fO_2 to be controlled and monitored at deep mantle pressures[71,94] will enable the stabilities of various

carbonate minerals to be mapped out as a function of depth for complex systems, combined with their predicted seismic velocities based on their crystal structure.[76] Future improvements in the sensitivity of remote-sensing tools and data processing may allow deep carbonated mantle regions to be detected. Recent studies indicate that Fe-bearing carbonates show remarkably complex chemical and physical behavior at mid-lower mantle depths. The Fe spin transition may shift the chemical equilibrium in favor of Fe-rich carbonates, which in turn would significantly affect their physical properties, with potential implications for carbonate seismic detectability. However, the relevant depth range of spin transitions is not well constrained because of the immense technological challenge of probing spin transitions at combined high-pressure, high-temperature conditions. The iron oxides, oxygen, and elemental carbon that may be produced during reactions that take place when carbonate is transported to the deep mantle may also affect redox conditions and have important (but as yet unexplored) geological consequences.

Acknowledgments

VS acknowledges financial support from the Deep Carbon Observatory and Sapienza University of Rome through "Fondi di Ateneo." SA is grateful for funding from the German Research Foundation (DFG) under grant AU 356/10. Thoughtful comments by the reviewer Arno Rohrbach and the editor Rajdeep Dasgupta helped to improve the quality of this chapter.

Questions for the Classroom

1 Describe the different ways in which carbon bonds with other elements. Which type of bonding is involved in the carbon phases discussed in this chapter? Can carbon bond with any element in the periodic table? Why or why not? Do you think there are any forms of carbon that have not yet been discovered?
2 Select one form of carbon that occurs on modern Earth's surface (e.g. dolomite) and follow its subduction journey in terms of the chemical reactions that take place involving its carbon atoms. Repeat the exercise for other carbon forms that are found on modern Earth's surface.
3 Repeat the previous exercise for the subduction of different forms of carbon in early Earth (at least 3 Ga).
4 Which of the chemical reactions in the two previous exercises are redox reactions? Describe how the cycles of other elements may be linked to the deep carbon cycle.
5 What is the estimated content of carbon in Earth as a function of depth? In which phases does carbon dominantly occur? Construct a histogram showing the variations of carbon phases and their abundance with depth. Now repeat the exercise showing only how the abundance of different oxidation states of carbon varies with depth.

6 Why is it so challenging to estimate the amount of carbon in Earth? Why does knowing how much carbon is present matter?
7 Are there any external manifestations of the deep carbon cycle on Earth's surface? Has this changed through geologic time?
8 How does the deep carbon cycle affect the habitability of modern Earth? Are there any links to climate change? Do any of the answers to these questions change if we consider early Earth?
9 Describe a high-pressure experiment that could help to answer some of the unknowns regarding carbon and its forms inside Earth.
10 Which types of natural samples could help to resolve these unknowns regarding carbon and its forms inside Earth? Note that the natural samples do not have to have been discovered yet.

References

1. Kasting, J.F., Eggler, D.H. & Raeburn, S.P. Mantle redox evolution and the oxidation state of the Archean atmosphere. *Journal of Geology*, **101**, 245–257 (1993).
2. McDonough, W.F. & Sun, S.-S. The composition of the Earth. *Chemical Geology*, **120**, 223–253 (1995).
3. Marty, B., Alexander, C.M.O. & Raymond, S. Primordial origins of Earth's carbon. *Reviews in Mineralogy and Geochemistry*, **75**, 149–181 (2013).
4. Keppler, H., Wiedenbeck, M., & Shcheka, S.S. Carbon solubility in olivine and the mode of carbon storage in the Earth's mantle. *Nature*, **424**, 414–416 (2003).
5. Rosenthal, A., Hauri, E. & Hirschmann, M. Experimental determination of C, F, and H partitioning between mantle minerals and carbonated basalt, CO_2/Ba and CO_2/Nb systematics of partial melting, and the CO_2 contents of basaltic source regions. *Earth and Planetary Science Letters*, **412**, 77–87 (2015).
6. Shcheka, S.S., Wiedenbeck, M., Frost, D.J. & Keppler, H. Carbon solubility in mantle minerals. *Earth and Planetary Science Letters*, **245**, 730–742 (2006).
7. Hayden, L.A. & Watson, E.B. Grain boundary mobility of carbon in Earth's mantle: a possible carbon flux from the core. *Proceedings of the National Academy of Sciences*, **105**, 8537–8541 (2008).
8. Ni, H. & Keppler, H. Carbon in silicate melts. *Reviews in Mineralogy and Geochemistry*, **75**, 251–287 (2013).
9. LeVoyer, M., Kelley, K., Cottrell, E. & Hauri, E. Heterogeneity in mantle carbon content from CO_2-undersaturated basalts. *Nature Communications*, **8**, 14062 (2017).
10. Saal, A.E., Hauri, E., Langmuir, C.H. & Perfit, M.R. Vapour undersaturation in primitive mid-ocean-ridge basalts and the volatile content of Earth's upper mantle. *Nature*, **419**, 451–455 (2002).
11. Dixon, J.E., Clague, D.A., Wallace, P. & Poreda, R. Volatiles in alkalic basalts from the north arc volcanic field, Hawaii: extensive degassing of deep submarine-erupted alkalic series lavas. *Journal of Petrology*, **38**, 911–939 (1997).
12. Li, Y., Dasgupta, R., Tsuno, K., Monteleone, B. & Shimizu, N. Carbon and sulfur budget of the silicate Earth explained by accretion of differentiated planetary embryos. *Nature Geoscience*, **9**, 781–785 (2016).

13. Frost, D.J., Mann, U., Asahara, Y. & Rubie, D.C. The redox state of the mantle during and just after core formation. *Philosophical Transactions of the Royal Society: Series A*, **366**, 4315–4337 (2008).
14. Scaillet, B. & Gaillard, F. Redox state of early magmas. *Nature*, **480**, 48–49 (2011).
15. Trail, D., Watson, E.B. & Tailby, N.D. The oxidation state of Hadean magmas and implications for early Earth's atmosphere. *Nature*, **480,** 79–82 (2011).
16. Li, Z.-X.A. & Lee, C.-T.A. The constancy of upper mantle fO_2 through time inferred from V/Sc ratios in basalts. *Earth and Planetary Science Letters*, **228**, 483–493 (2004).
17. Aulbach, S. & Stagno V. Evidence for a reducing Archean ambient mantle and its effects on the carbon cycle. *Geology*, **44**, 9 (2016).
18. Stagno, V., Ojwang, D.O., McCammon, C.A. & Frost, D.J. The oxidation state of the mantle and the extraction of carbon from Earth's interior. *Nature*, **493**, 84–88 (2013).
19. Stagno, V. & Frost D.J. Carbon speciation in the asthenosphere: experimental measurements of the redox conditions at which carbonate-bearing melts coexist with graphite or diamond in peridotite assemblages. *Earth and Planetary Science Letters*, **30**, 72–84 (2010).
20. Dasgupta, R. Ingassing, storage, and outgassing of terrestrial carbon through geologic time. *Reviews in Mineralogy and Geochemistry*, **75**, 183–229 (2013).
21. Aulbach, S. & Viljoen, K.S. Eclogite xenoliths from the Lace kimberlite, Kaapvaal craton: from convecting mantle source to palaeo-ocean floor and back. *Earth and Planetary Science Letters*, **431**, 274–286 (2015).
22. Ballhaus, C. & Frost, B.R. The generation of oxidized CO_2-bearing basaltic melts from reduced CH_4-bearing upper mantle sources. *Geochimica et Cosmochimica Acta*, **58**, 4931–4940 (1994).
23. Sorbadere, F., Laurenz, V., Frost, D.J., Wenz, M., Rosenthal, A., McCammon, C.A. & Rivard, C. The behaviour of ferric iron during partial melting of peridotite. *Geochimica et Cosmochimica Acta*, **239**, 235–254 (2018).
24. Aulbach, S., Jacob, D.E., Cartigny, P., Stern, R.A., Simonetti, S.S. & Viljoen, K.S. Eclogite xenoliths from Orapa: ocean crust recycling, mantle metasomatism and carbon cycling at the western Zimbabwe craton margin. *Geochimica et Cosmochimica Acta*, **213**, 574–592 (2017).
25. Nicklas, R.W., Puchtel, I.S. & Ash, R. Redox state of the Archean mantle: evidence from V partitioning in 3.5–2.4 Ga Komatiites. *Geochimica et Cosmochimica Acta*, **222**, 447–466 (2018).
26. Stagno V., Frost, D.J., McCammon, C.A., Mohseni, H. & Fei, Y. The oxygen fugacity at which graphite or diamond forms from carbonate-bearing melts in eclogitic rocks. *Contributions to Mineralogy and Petrology*, **169**, 16 (2015).
27. Ballhaus, C., Berry, R.F. & Green, D.H. High pressure experimental calibration of the olivine–orthopyroxene–spinel oxygen geobarometer: implications for the oxidation state of the upper mantle. *Contributions of Mineralogy and Petrology*, **107**, 27–40 (1991).
28. Garber, J.M. et al. Multidisciplinary constraints on the abundance of diamond and eclogite in the cratonic lithosphere. *Geochemistry, Geophysics, Geosystems*, **19**, 2062–2086 (2018).
29. Woolley, A.R. & Kjarsgaard, B.A. Carbonatite Occurrences of the World: Map and Database; *Geological Survey of Canada*, Open File 5796, 1 CD-ROM + 1 map (2008).
30. Tappe, S., Romer, R.L., Stracke, A., Steenfelt, A., Smart, K.A., Muehlenbachs, K. & Torsvik, T.H. Sources and mobility of carbonate melts beneath cratons, with

implications for deep carbon cycling, metasomatism and rift initiation. *Earth and Planetary Science Letters*, **466**, 152–167 (2017).
31. Tappe, S., Smart, K., Torsvik, T., Massuyeau, M. & de Wit, M. Geodynamics of kimberlites on a cooling Earth: clues to plate tectonic evolution and deep volatile cycles. *Earth and Planetary Science Letters*, **484**, 1–14 (2018).
32. Aulbach, S., Woodland, A.B., Vasilyev, P., Galvez, M.E. & Viljoen, K.S. Effects of low-pressure igneous processes and subduction on $Fe^{3+}/\sum Fe$ and redox state of mantle eclogites from Lace (Kaapvaal craton). *Earth and Planetary Science Letters*, **474**, 283–295 (2017).
33. Dasgupta, R. & Hirschmann, M.M. The deep carbon cycle and melting in Earth's interior. *Earth and Planetary Science Letters (Frontiers)*, **298**, 1–13 (2010).
34. Rohrbach, A., Ghosh, S., Schmidt, M.W., Wijbrans, C.H. & Klemme, S. The stability of Fe–Ni carbides in the Earth's mantle: evidence for a low Fe–Ni–C melt fraction in the deep mantle. *Earth and Planetary Science Letters*, **388**, 211 (2014).
35. Luth, R.W. Diamonds, eclogites and the oxidation state of the Earth's mantle. *Science*, **261**, 66–68 (1993).
36. McDonough, W.F. & Sun, S.-S. The composition of the Earth. *Chemical Geology*, **120**, 223–253 (1995).
37. Eguchi, J. & Dasgupta, R. Redox state of the convective mantle from CO_2-trace element systematics of oceanic basalts. *Geochemical Perspectives Letters,* **8**, 17–21 (2018).
38. Frost, D.J., Liebske, C., Langenhorst, F. & McCammon, C.A. Experimental evidence for the existence of iron-rich metal in the Earth's lower mantle. *Nature*, **428**, 409–412 (2004).
39. Rohrbach, A., Ballhaus, C., Ulmer, P., Golla-Schindler, U. & Schönbohm, D. Experimental evidence for a reduced metal-saturated upper mantle. *Journal of Petrology*, **52**, 717–731 (2011).
40. Smith, E.M., Shirey, S., Nestola, F., Bullock, E.S., Wang, J., Richardson, S. & Wang, W. Large gem diamonds from metallic liquid in Earth's deep mantle. *Science*, **354**, 1403–1405 (2016).
41. Jacob, D.E. Nature and origin of eclogite xenoliths from kimberlites. *Lithos*, **77**, 295–316 (2004).
42. Kaminsky, F.V. & Wirth, R. Iron carbide inclusions in lower-mantle diamond from Juina, Brazil, *Canadian Mineralogist*, **49**, 555–572 (2011).
43. Mikhail, S. et al. Empirical evidence for the fractionation of carbon isotopes between diamond and iron carbide from the Earth's mantle. *Geochemistry, Geophysics, Geosystems*, **15**, 855–866 (2014).
44. Schmidt, M.W., Gao, C., Golubkova, A., Rohrbach, A. & Connolly, J.A.D. Natural moissanite (SiC) – a low temperature mineral formed from highly fractionated ultra-reducing COH-fluids. *Progress in Earth and Planetary Science*, **1**, 27 (2014).
45. Palyanov, Y.N., Bataleva, Y.V., Sokol, A.G., Borzdov, Y.M., Kupriyanov, I.N., Reutsky, V.N. & Sobolev, N.V. Mantle–slab interaction and redox mechanism of diamond formation. *Proceedings of the National Academy of Sciences*, **110**, 20408–20413 (2013).
46. Tsuno, K. & Dasgupta, R. Fe–Ni–Cu–C–S phase relations at high pressures and temperatures – the role of sulfur in carbon storage and diamond stability at mid- to deep-upper mantle. *Earth and Planetary Science Letters*, **412**, 132–142 (2015).
47. Brenker, F.E. et al. Carbonates from lower part of transition zone or even the lower mantle. *Earth and Planetary Science Letters*, **260**, 1–9 (2007).

48. Kaminsky, F.V., Ryabchikov, I.D. & Wirth, R. A primary natrocarbonatitic association in the deep Earth. *Mineralogy and Petrology*, **110**, 387–398 (2016).
49. Hammouda, T. & Keshav, S. Melting in the mantle in the presence of carbon: review of experiments and discussion on the origin of carbonatites. *Chemical Geology*, **418**, 171–188 (2015).
50. Santillan, J., Williams, Q. & Knittle, E. Dolomite-II: a high-pressure polymorph of $CaMg(CO_3)_2$. *Geophysical Research Letters*, **30**, 2 (2003).
51. Mao, Z., Armentrout, M., Rainey, E., Manning, C.E., Dera, P., Prakapenka, V.B. & Kavner A. Dolomite III: a new candidate lower mantle carbonate. *Geophysical Research Letters*, **38**, L22303 (2011).
52. Merlini, M., Crichton, W., Hanfland, M., Gemmi, M., Mueller, H., Kupenko, I. & Dubrovinsky, L. Dolomite-II and dolomite-III: crystal structures and stability in the Earth's lower mantle. *Proceedings of the National Academy of Sciences*, **109**, 13509–13514 (2012b).
53. Merlini, M. et al. Dolomite-IV: candidate structure for a carbonate in the Earth's lower mantle. *American Mineralogist*, **102**, 1763–1766 (2017).
54. Dorfman, S.M., Badro, J., Nabiei, F., Prakapenka, V.B., Cantoni, M. & Gillet, P. Carbonate stability in the reduced lower mantle. *Earth and Planetary Science Letters*, **489**, 84 (2018).
55. Liu, Y. et al. First direct evidence of sedimentary carbonate recycling in subduction-related xenoliths. *Scientific Reports*, **5**, 11547 (2015).
56. Merlini, M., Hanfland, M., & Crichton, W. $CaCO_3$-III and $CaCO_3$-VI, high-pressure polymorphs of calcite: possible host structures for carbon in the Earth's mantle. *Earth and Planetary Science Letters*, **333–334**, 265–271 (2012).
57. Ono, S., Kikegawa, T. & Ohishi, Y. High-pressure transition of $CaCO_3$. *American Mineralogist*, **92**, 1246–1249 (2007).
58. Oganov, A.R., Glass, C.W., & Ono, S. High-pressure phases of $CaCO_3$: crystal structure prediction and experiment. *Earth and Planetary Science Letters*, **241**, 95–103 (2006).
59. Pickard, C.J. & Needs, R.J. Structures and stability of calcium and magnesium carbonates at mantle pressures. *Physical Review B*, **91**, 104101 (2015).
60. Lobanov, S.S. et al. Raman spectroscopy and X-ray diffraction of sp^3 $CaCO_3$ at lower mantle pressures. *Physical Review B*, **96**, 104101 (2017).
61. Cerantola, V. et al. High-pressure spectroscopic study of siderite ($FeCO_3$) with a focus on spin crossover. *American Mineralogist*, **100**, 2670–2681 (2015).
62. Lobanov, S.S., Goncharov, A.F. & Litasov, K.D. Optical properties of siderite ($FeCO_3$) across the spin transition: crossover to iron-rich carbonates in the lower mantle. *American Mineralogist*, **100**, 1059–1064 (2015).
63. Lobanov, S.S., Holtgrewe, N. & Goncharov, A.F. Reduced radiative conductivity of low spin FeO_6-octahedra in $FeCO_3$ at high pressure and temperature. *Earth and Planetary Science Letters*, **449**, 20–25 (2016).
64. Isshiki, M. et al. Stability of magnesite and its high-pressure form in the lowermost mantle. *Nature*, **427**, 60–63 (2004).
65. Solopova, N.A. et al. Melting and decomposition of $MgCO_3$ at pressures up to 84 GPa. *Physics and Chemisrty of Minerals*, **42**, 73–81 (2014).
66. Maeda, F., Ohtani, E., Kamada, S., Sakamaki, T., Hirao, N. & Ohishi, Y. Diamond formation in the deep lower mantle: A high-pressure reaction of $MgCO_3$ and SiO_2. *Scientific Reports*, **7**, 40602 (2017).

67. Cerantola, V. et al. Stability of iron-bearing carbonates in the deep Earth's interior. *Nature Communications*, **8**, 15960 (2017).
68. Kang, N. et al. Melting of siderite to 20 GPa and thermodynamic properties of $FeCO_3$-melt. *Chemical Geology*, **400**, 34–43 (2015).
69. Boulard, E. et al. New host for carbon in the deep Earth. *Proceedings of the National Academy of Sciences*, **108**, 5184–5187 (2011).
70. Merlini, M., Hanfland, M., Salamat, A., Petitgirard, S. & Müller, H. The crystal structures of $Mg_2Fe_2C_4O_{13}$, with tetrahedrally coordinated carbon, and Fe13O19, synthesized at deep mantle conditions. *American Mineralogist*, **100**, 2001–2004 (2015).
71. Stagno, V., Tange, Y., Miyajima, N., McCammon, C.A., Irifune, T. & Frost, D.J. The stability of magnesite in the transition zone and the lower mantle as function of oxygen fugacity. *Geophysical Research Letters*, **38**, L19309 (2011).
72. McCammon, C. Microscopic properties to macroscopic behavior: the influence of iron electronic states. *Journal of Mineralogical and Petrological Science*, **101**, 130–144 (2006).
73. Kiseeva, E. et al. Oxidized iron in garnets from the mantle transition zone. *Nature Geoscience*, **11**, 144–147 (2018).
74. Beyer, C. & Frost, D.J. The depth of sub-lithospheric diamond formation and the redistribution of carbon in the deep mantle. *Earth and Planetary Science Letters*, **461**, 30–39 (2017).
75. Ismailova, L. et al. Stability of Fe,Al-bearing bridgmanite in the lower mantle and synthesis of pure Fe-bridgmanite. *Science Advances*, **2**, e1600427 (2016).
76. Sanchez-Valle, C., Ghosh S. & Rosa A.D. Sound velocities of ferromagnesian carbonates and the seismic detection of carbonates in eclogites and the mantle. *Geophysical Research Letters*, **38**, L24315 (2011).
77. Yang, J., Mao, Z., Lin, J.-F. & Prakapenka, V. Single-crystal elasticity of the deep-mantle magnesite at high pressure and temperature. *Earth and Planetary Science Letters*, **392**, 292–299 (2014).
78. Mattila, A. et al. Pressure induced magnetic transition in siderite $FeCO_3$ studied by X-ray emission spectroscopy. *Journal of Physics: Condensed Matter*, **19**, 386206 (2007).
79. Shi, H., Luo, W., Johansson, B. & Ahuja, R. First-principles calculations of the electronic structure and pressure-induced magnetic transition in siderite $FeCO_3$. *Physical Review B*, **78**, 155119 (2008).
80. Lavina, B., Dera, P., Downs, R.T., Prakapenka, V., Rivers, M., Sutton, S. & Nicol, M. Siderite at lower mantle conditions and the effects of the pressure-induced spin-pairing transition. *Geophysical Research Letters*, **36**, L23306 (2009).
81. Lavina, B. et al. Structure of siderite $FeCO_3$ to 56 GPa and hysteresis of its spin-pairing transition. *Physical Review B*, **82**, 064110 (2010b).
82. Lin, J.-F., Liu, J., Jacobs, C. & Prakapenka, V.B. Vibrational and elastic properties of ferromagnesite across the electronic spin-pairing transition of iron. *American Mineralogist*, **97**, 583–591 (2012).
83. Farfan, G., Wang, S., Ma, H., Caracas, R. & Mao, W.L. Bonding and structural changes in siderite at high pressure. *American Mineralogist*, **97**, 1421–1426 (2012).
84. Cerantola, V. et al. High-pressure spectroscopic study of siderite ($FeCO_3$) with a focus on spin crossover. *American Mineralogist*, **100**, 2670–2681 (2015).

85. Lobanov, S.S., Goncharov, A.F. & Litasov, K.D. Optical properties of siderite ($FeCO_3$) across the spin transition: crossover to iron-rich carbonates in the lower mantle. *American Mineralogist*, **100**, 1059–1064 (2015).
86. Weis, C. et al. Pressure driven spin transition in siderite and magnesiosiderite single crystals. *Scientific Reports*, **7**, 16526 (2017).
87. Liu, J., Lin, J.F., Mao, Z., & Prakapenka, V.B. Thermal equation of state and spin transition of magnesiosiderite at high pressure and temperature. *American Mineralogist*, **99**, 84–93 (2014).
88. Fu, S., Yang, J. & Lin, J.F. Abnormal elasticity of single-crystal magnesiosiderite across the spin transition in Earth's lower mantle. *Physical Reviews Letters*, **118**, 036402 (2017).
89. Stekiel, M. et al. High pressure elasticity of $FeCO_3$–$MgCO_3$ carbonates. *Physics of the Earth and Planetary Interiors*, **271**, 57–63 (2017).
90. Müller, J., Efthimiopoulos, I., Jahn, S. & Koch-Müller, M. Effect of temperature on the pressure-induced spin transition in siderite and iron-bearing magnesite: a Raman spectroscopy study. *European Journal of Mineralogy*, **29**, 785–793 (2017).
91. Kono, Y. et al. Ultralow viscosity of carbonate melts at high pressure. *Nature Communications*, **5**, 5091 (2014).
92. Stagno, V., Stopponi, V., Kono, Y., Manning, C.E. & Irifune T. Experimental determination of the viscosity of Na_2CO_3 melt between 1.7 and 4.6 GPa at 1200–1700 °C: implications for the rheology of carbonatite magmas in the Earth's upper mantle. *Chemical Geology*, **501**, 19–25 (2018).
93. Frost, D.J. & McCammon, C.A. The redox state of the Earth's mantle. *Annual Review of Earth and Planetary Science*, **36**, 389–420 (2008).
94. Rohrbach, A. & Schmidt, M.W. Redox freezing and melting in the Earth's deep mantle resulting from carbon–iron redox coupling. *Nature*, **472**, 209–212 (2011).
95. O'Reilly, S.Y. & Griffin, W.L. Moho vs crust–mantle boundary: evolution of an idea. *Tectnophysics*, **609**, 535–546 (2013).
96. Foley, S.F. A reappraisal of redox melting in the Earth's mantle as a function of tectonic setting and time. *Journal of Petrology*, **52**, 1363–1391 (2011).
97. Gaillard, F., Scaillet, B., Pichavant, M. & Iacono-Marziano, G. The redox geodynamics linking basalts and their mantle sources through space and time. *Chemical Geology*, **418**, 217–233 (2015).
98. Litasov, K.D. & Shatskiy, A. Carbon-bearing magmas in the Earth's deep interior. In: Kono, Y. & Sanloup, C. (eds.), *Magmas under Pressure: Advances in High-Pressure Experiments on Structure and Properties of Melts*. Amsterdam: Elsevier, pp. 43–82 (2018).
99. Sakamaki, T. Structure and properties of silicate magmas. In: Kono, Y. & Sanloup, C. (eds.), *Magmas under Pressure: Advances in High-Pressure Experiments on Structure and Properties of Melts*. Amsterdam: Elsevier, pp. 323–341 (2018).
100. Sifre', D., Gardes, E., Massuyeau, M., Hashim, L., Hier-Majumder, S. & Gaillard, F. Electrical conductivity during incipient melting in the oceanic low-velocity zone. *Nature*, **509**, 81–85 (2014).